Band alignments at Ga_2O_3 heterojunction interfaces with Si and Ge

J. T. Gibbon[1,2], L. Jones[1,2,3], J. W. Roberts[4], M. Althobaiti[5], P. R. Chalker[4], Ivona Z. Mitrovic[3], V. R. Dhanak[1,2*]

[1] *Stephenson Institute for Renewable Energy, University of Liverpool, Chadwick Building, Peach Street, Liverpool, L69 7ZF, United Kingdom*

[2] *Department of Physics, University of Liverpool, Oliver Lodge Building, Oxford Street, Liverpool, L69 7ZE, United Kingdom*

[3] *Department of Electrical Engineering and Electronics, University of Liverpool, Brownlow Hill, Liverpool, L69 3GJ, United Kingdom*

[4] *School of Engineering, University of Liverpool, Brownlow Hill, Liverpool, L69 3GH, United Kingdom*

[5] *Department of Physics, Faculty of Science, Taif University, Taif 888, Saudi Arabia*

Amorphous Ga_2O_3 thin films were deposited on p-type (111) and (100) surfaces of silicon and (100) germanium by atomic layer deposition (ALD). X-ray photoelectron spectroscopy (XPS) was used to investigate the band alignments at the interfaces using the Kraut Method. The valence band offsets were determined to be 3.49± 0.08 eV and 3.47± 0.08 eV with Si(111) and Si(100) respectively and 3.51eV± 0.08 eV with Ge(100). Inverse photoemission spectroscopy (IPES) was used to investigate the conduction band of a thick Ga_2O_3 film and the band gap of the film was determined to be 4.63±0.14 eV. The conduction band offsets were found to be 0.03 eV and 0.05eV with Si(111) and Si(100) respectively, and 0.45eV with Ge(100). The results indicate that the heterojunctions of Ga_2O_3 with Si(100), Si(111) and Ge(100) are all type I heterojunctions.

Ga_2O_3 is a wide band gap material with the largest band gap of the transparent conducting oxides, at ≈4.8 eV. The large band gap, combined with the excellent thermal and chemical stabilities of the material have led to considerable recent interest in the material, for applications as wide ranging as gas-sensing[1–3], high-power electronics[4], photovoltaics[5,6] and UV optoelectronics[7–9]. A Ga_2O_3 metal-oxide-semiconductor capacitor has also recently been reported on silicon[10], as has the use of ALD-grown Ga_2O_3 as an ultrathin passivation layer for silicon-based photovoltaics[6].

To understand the behaviour of these devices, the band alignments with commonly used semiconductor substrates need to be investigated. The band alignment of β-Ga_2O_3 with Si has previously been reported by Guo *et al.*[9] using the electron affinity rule[11], however this disagrees with the alignment obtained by Chen *et al.*[12], where the alignment is measured by photoelectron spectroscopy. The interpretation of the alignment obtained by Chen *et al.* is complicated by a number of issues: Firstly, the authors use a non-monochromatic x-ray source, resulting in the presence of x-ray satellites, which are particularly problematic for finding the valence band maximum (VBM) of the Ga_2O_3 sample; secondly, the interfacial sample is produced by Ar^+ ion etching, however, the interfacial sample clearly shows two Ga species in

* Author to whom correspondence should be addressed. Electronic mail: V.R.Dhanak@liverpool.ac.uk

the Ga 2p spectrum, indicative of the preferential removal of oxygen, thus leaving a sub-stoichiometric oxide or elemental Ga; finally, their discussion on the formation of an interfacial SiO_{2-x} layer is limited by the issues raised above.

The band offsets of Ga_2O_3 with Ge have not been reported previously, with only that found for $Ga_2O_3(Gd_2O_3)$ having been reported, where $\Delta E_v = 2.35 \pm 0.1$ eV[13], however in this case the Kraut method is used incorrectly, as the thickest sample used is only 3 nm and therefore still sensitive to the interface. Previous reports of photoelectron spectroscopy on $Ga_2O_3(Gd_2O_3)$ on Ge have found evidence of an interfacial oxide layer formed upon deposition of the dielectric layer[14,15], with the notable exception of Chu *et al.*[13], however the binding energy reported is considerably larger (at a binding energy of approximately 30 eV) than that expected for elemental Ge. Such an energy suggests that the wafer may in fact be oxidized, however accurate determination of the oxidation state is rendered impossible since the data had not been deconvoluted.

In this work, we describe the use of the Kraut method[16] to investigate the band alignments of Ga_2O_3 with Si(111), Si(100) and Ge(100) substrates. As the Kraut method requires a thick, bulk-like sample, a thin, interfacial sample, where the core-levels of the substrate can be observed and a clean substrate, thick (31 nm) and thin (3 nm) Ga_2O_3 layers were synthesized on the aforementioned substrates. Regarding the thickness, the Debye length is characteristic of the length scale over which the effect of the interfacial potential is felt. For crystalline β-Ga_2O_3 nanowires, the Debye length is found to be 40.5 nm[17]. However, as the Debye length is proportional to the defect density[18], the Debye length of the films described here will be considerably smaller, as the films described in this work are amorphous and hence defect-rich. Similar behaviour has been observed in a-IGZO thin film transistors[18], where the defect density is approximately $2 \times 10^{17} \mathrm{cm}^{-3}$. Hence, the thickness of the 31 nm samples used in this work is considered adequate.

The use of a thin sample also allows for the quality of the interface to be investigated in a non-destructive manner. In contrast to Chen *et al.*[12], we use a monochromatic x-ray source, thus avoiding the issue of x-ray satellites.

Ga_2O_3 layers were deposited by atomic layer deposition (ALD) on clean p-type Si(111) and Ge(100) wafers in an Oxford Instruments Plasma-OpAL reactor. The precursors used for deposition were triethylgallium (TEGa) and O_2 plasma and with a substrate temperature of 250˚C. 58 ALD cycles were used to obtain thin samples, and 580 cycles for the thick samples.

Prior to deposition, the Si substrates were cleaned by 10 minutes immersed in methanol in a sonic bath, followed by 10 minutes immersed in acetone in a sonic bath. The Si substrates were then immersed in 5% HF for 5 minutes with agitation before being rinsed with distilled water and dried by N_2 gas. The Ge substrates were cleaned by 10 minutes immersed in methanol in a sonic bath, followed by 10 minutes immersed in acetone in a sonic bath and dried by N_2 gas.

X-ray photoelectron spectroscopy (XPS) measurements were performed in a standard UHV chamber, with a base pressure below 2×10^{-10} mbar, with the main residual gas being hydrogen. A monochromatic Al Kα SPECS XR 50 M source ($h\nu = 1486.6$ eV) operating at a nominal power of 250 W was used in conjunction with a PSP Vacuum Technology Ltd Resolve 120 MCD5 electron energy analyzer. The spectrometer was calibrated to the positions of the Ag $3d_{5/2}$ and Fermi level of a clean polycrystalline Ag foil. By fitting the Fermi-Dirac distribution to the Ag Fermi level, the resolution of the analyzer is found to be 0.37±0.05 eV. Spectra are charge-corrected to the C 1s peak at 285.00 eV, due to adsorbed, adventitious carbon.

Inverse photoemission spectroscopy measurements were performed using a PSP Vacuum Technology BaO cathode dispenser electron source and an isochromat NaCl photon detector, both at 45˚ to the sample normal. Energy calibration was performed using the known energy position of the lowest unoccupied molecular orbital of multilayer C60 deposited in situ and the spectrometer resolution determined from a polycrystalline Ag foil was 1.00±0.10 eV.

The deposited films were confirmed to be amorphous by x-ray diffraction with a Rigaku SmartLab x-ray diffractometer ($h\nu = 8047.8$ eV). Spectroscopic ellipsometry was used to determine the thicknesses of the deposited films with a Horbia Jobin Yvon MM-16 spectrometer with a range of 430 – 850 nm. The thicknesses of the deposited films were found to be 30.05±0.18 nm and 3.05±0.10 nm for the thick and thin layers respectively. Ellipsometry spectra were fitted using a Cauchy model adopted from Ref [19].

The XPS spectra were analysed using the CasaXPS software. Core-levels were fitted with pseudo-Voigt functions atop a Shirley background. Valence band maxima (VBM) positions were found by linear extrapolation to the background. The errors on core-level binding energies and the VBM were determined to be ±0.05 eV. Since the mean-free-path of the photoelectrons is dependent on the kinetic energy of the emitted photoelectron, core-levels with large separations in kinetic energy will have different probing depths and hence different sensitivities to the interface potential. The Ga 3p, Ge 3p and Si 2p core-levels were therefore used for Kraut method analysis as these peaks occur in a narrow range of binding energies, ensuring that the photoelectrons originated from similar depths.

The Kraut method, uses the binding energies of the core levels and the VBM of the three samples to determine the valence band offset (VBO), ΔE_v, as shown in equation (1)

$$\Delta E_v = \Delta E_{CL} + (E_c^A - \xi^A)_{sub} - (E_c^B - \xi^B)_{thick} \quad (1)$$

Where $\Delta E_{CL} = E_{thin}^B - E_{thin}^A$ is the energy difference between the core levels of the deposited film and the substrate for the 3 nm sample, and ξ denotes the VBM for the relevant sample.

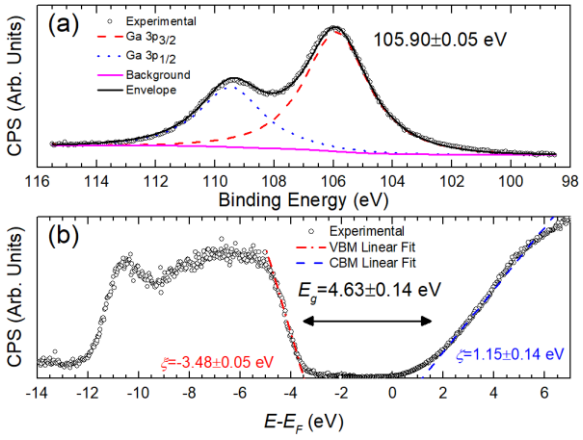

Fig. 1 – This figure shows (a) the Ga 3p core levels, and (b) the valence band obtained by XPS and the conduction band edge obtained by IPES for the 30nm Ga_2O_3 sample.

Fig. 1(a) show the Ga 3p region for the thick, 30 nm Ga_2O_3 sample. Fig. 1(b) shows the valence band measured by XPS and the conduction band, as measured by IPES. The VBM was found at -3.48±0.05 eV, whilst the CBM occurred at 1.15±0.14 eV relative to the Fermi level. By combining these values, the bandgap of the 30 nm Ga_2O_3 film was determined to be 4.63±0.14 eV, consistent with the 4.4-4.9 eV band gap range previously reported for amorphous Ga_2O_3 films[20–23].

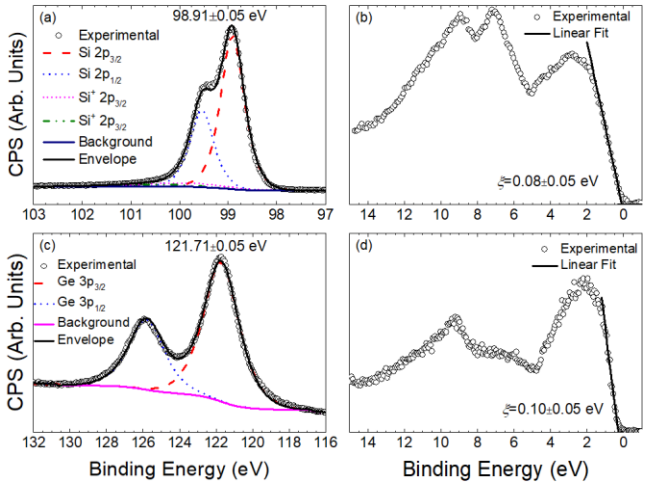

Fig. 2- (a) shows the Si 2p region for the clean Si(111) substrate (b) shows the corresponding valence band. (c) shows the clean Ge 3p for the Ge(100) substrate and (d) shows the valence band for the same sample.

Fig. 2(a) and Fig. 2(b) shows the Si 2p region and valence band respectively for the clean Si(111) substrate. Fig. 2(c) and Fig. 2(d) show the Ge 3p region and valence band for the clean Ge(100) substrate. The data show that the surfaces of the substrates were clean of any contamination. The binding energies and their differences from the VBM obtained from these figures are given in table I. The binding energy of the Si $2p_{3/2}$ core-level is consistent with values reported in the literature for p-type Si wafers[24–27]. The separation between the Si $2p_{3/2}$ and the VBM is found to be 98.83±0.08 eV, consistent with that reported previously[27–30].

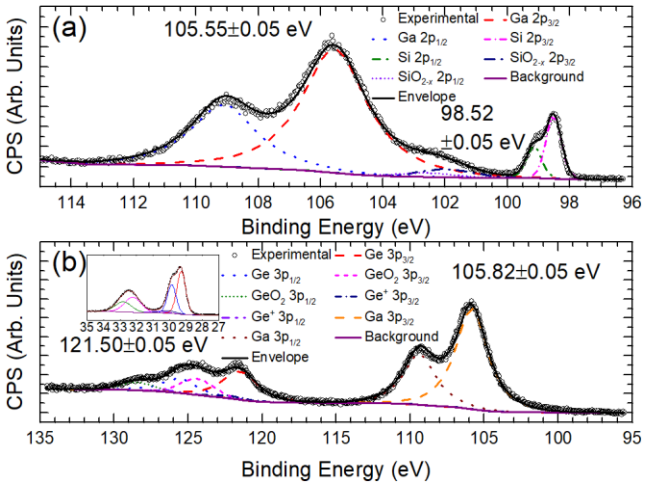

Fig. 3-(a) shows the Si 2p and Ga 3p region for the interfacial Ga_2O_3/Si(111) sample. (b) shows the Ge 3p and Ga 3p region for the interfacial Ga_2O_3/Ge(100) sample. Inset is the Ge 3d spectrum as measured by XPS.

Fig. 3(a) shows the Si 2p and Ga 3p region for the 3 nm Ga_2O_3/Si(111) sample, whilst Fig. 3(b) shows the Ge 3p and Ga 3p region for the 3 nm Ga_2O_3/Ge(100) sample.

As XPS is a surface-sensitive technique, varying the take-off angle will change the effective probing depth for a particular photon energy. The dependence of the mean-free-path of the photoelectrons in the material on the take-off angle is given by $\lambda = \lambda_0 \sin\theta$, where λ_0 is the inelastic mean-free-path (IMFP) of an electron with the same kinetic energy, E, with a take-off angle normal to the sample surface, and is

calculated from $\lambda_0 = \frac{1430}{E^2} + 0.54\sqrt{E}$,[31,32] where E is in eV and λ_0 is in Å. Using this relation, the IMFP is calculated to be 2.0 nm. By measuring the core levels at multiple take-off angles, the presence of any band-bending close to the interface can be determined. The Ga $3p_{3/2}$, Si $2p_{3/2}$ and Ge $3p_{3/2}$ binding energies were determined for 30˚, 60˚ and 90˚ take-off angles. If band-bending were present at the interface, it would be expected that the difference in the core-level binding energies, ΔE_{CL} would vary with different take off angles. In fact, no such angular dependence is seen, as shown in Fig. 4(a)-(c). It can, therefore, be concluded that band bending at the interface is negligible for these systems. If band-bending were present, then the FWHM of the core-levels would also be expected to broaden[33,34], in fact, no changes in the FWHM are observed, further confirming the absence of band-bending.

TABLE I -The binding energies positions of the core-levels and valence band minima and band gaps for each substrate and the bulk like Ga2O3. Also shown are the calculated valence band and conduction band offsets.

Substrate	E_B (eV)	ξ (eV)	E_g (eV)	E_B-ξ (eV)	ΔE_{CL} (eV)	ΔE_v (eV)	ΔE_c (eV)
Ge(100)	121.71	0.10	0.67	121.61	-15.68	-3.51	0.45
Si(111)	98.91	0.08	1.11	98.83	7.03	-3.49	0.03
Si(100)	98.92	0.13	1.11	98.79	7.10	-3.47	0.05
30 nm Ga_2O_3	105.90	3.48	4.63	102.42	-	-	-

By applying equation (1), the VBO for the amorphous Ga_2O_3 film on Si(111) was determined to be 3.49±0.08 eV consistent with that found for β-Ga_2O_3 on Si(111) by Chen *et al.* [12] and contrasting to that reported by Guo *et al*. [9]. The VBO for the amorphous Ga_2O_3 film on Ge(100) is likewise determined to be 3.51±0.08 eV.

Using the bandgap determined in Fig. 1(b) combined with literature bandgaps for Si(1.11 eV) and Ge (0.67 eV), the conduction band offsets (CBO) are found to be 0.03±0.14 eV and 0.45±0.14 eV for the Si(111) and Ge(100) samples respectively. The core-level energies, valence band maxima, band gaps and band offsets are summarised in table I. A schematic diagram of the band alignments is given in Fig. 4.

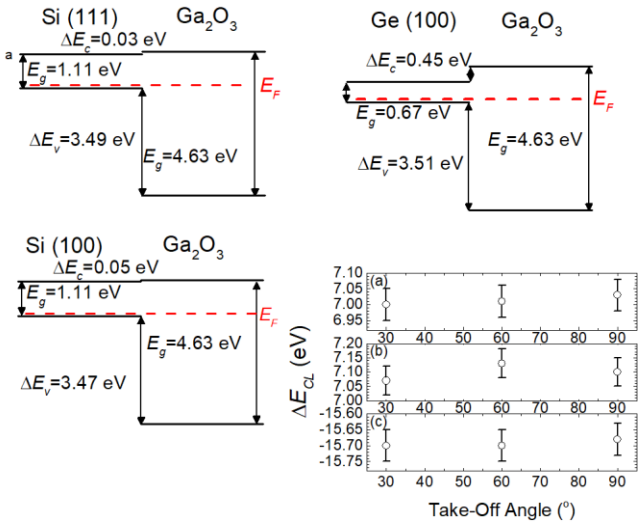

Fig. 4 – A schematic band alignment diagram showing the XPS determined band alignments for ALD-grown Ga_2O_3 on a variety of common semiconductor substrates. (a)-(c) show the difference in the core-level binding energies against the take-off angle for the Si(111), Si(100) and Ge(100) samples respectively. No difference above the error is observed, thus ruling out significant band-bending.

Similar measurements were also performed on a Si(100) substrate, the results of which are shown in table 1 and Fig. 4. The differences in the VBOs for the Si substrates are within the experimental error of the

XPS system. The VBOs obtained from both the Si(111) and Si(100) samples are consistent with that found by Chen *et al.*[12]. The CBOs obtained from the Si(111) and (100) are different to those obtained by Chen *et al.*[12], these differences are likely due to the different methods of evaluating the band gap. Chen *et al.* use the photoelectron energy loss spectrum (PEELS) from the O 1s peak, rather than the combined VBM-CBM separation used in this work. The error on the PEELS method can be estimated to be of the order of 0.6-1.0 eV from Figure 1b of Chen *et al.*[12]. An interesting question would be whether the doping level affects the band alignment. By considering the position of the VBM with respect to the Fermi level, we can conclude that the Si wafers used in this work are more heavily p-type doped than those used by Chen *et al.*[12], however the VBOs found are consistent, suggesting that the doping density has little effect on the band offsets.

Another important variable in the performance of semiconductor devices is the quality of the interface and the existence of any interfacial layers between the substrate and the deposited film. The substrate is frequently observed to be partially oxidized after deposition of a binary metal-oxide upon Si or Ge [29,35–43], but is typically less than 3 nm in thickness[10]. Fig. 3a shows the interfacial Si 2p and Ga 3p spectra. A second set of peaks attributed to silicon occur at 3.5 eV above the Si^0 $2p_{3/2,}$ consistent with that expected for the Si^{4+} oxidation state of SiO_2[44–47]. A similar layer was also observed for 3 nm Ga_2O_3/Si(100). Paskaleva *et al.*[10] have likewise observed the formation of an interfacial SiO_2 layer by ellipsometry and C-V measurements when depositing β-Ga_2O_3 on Si(100) by the closely related chemical vapour deposition technique. Chen *et al*[12]. do not observe this oxide formation, however the interpretation of their data is limited as the spectra presented are at low resolution and are not deconvoluted. The interpretation of their data is further complicated by the Ar^+ ion etching process used to produce the interfacial dataset. Here, the Ga 2p peaks are clearly asymmetric, suggesting the formation of either a non-stoichiometric oxide (Ga_2O_{3-x}, GaO), or possibly metallic Ga^0. These features would obscure the signal from the Si 2p for the interfacial oxide, as the Ga 3p peaks would be shifted to a similar binding energy as Si 2p from SiO_2. Interpretation of the spectra in Chen *et al.*[12] is further complicated by their use of a non-monochromatic x-ray source, resulting in x-ray satellite features. For a Mg source such as the one they used, these occur 8.4 eV and 10.1 eV away from the main peak on the low binding energy side[48]. An alternative explanation could be in the differences between the growth techniques as Chen *et al.*[12] used pulsed laser deposition to deposit their films, rather than the chemical techniques described here and by Paskaleva *et al.*[10].

Similarly, figure Fig. 3(b) shows the XPS spectrum for the interfacial Ga_2O_3/Ge(100) sample in the Ge 3p and Ga 3p region. Here, the formation of GeO_2 occurs analogous to the formation of SiO_2 above. The inset in figure Fig. 3(b) shows the Ge 3d region. As well as the GeO_2 previously mentioned, there is also a doublet shifted from the elemental Ge peaks by 0.80 eV. This corresponds to an oxidation state of Ge^+ [47].

The thickness of the interfacial oxide can be estimated by the process established by Hill *et al.*[49–51], where the thickness of the native oxide, *d*, is given by equation (2). I_o is the native oxide peak intensity, and I_s is the substrate peak intensity.

$$d = \lambda_0 \sin\theta \ln\left(1 + \frac{I_o}{I_s}\right) \quad (2)$$

Hence, by using equation (2), the native oxide thickness is found to be 0.73 nm, 0.75 nm, and 0.89 nm for the Si(111), Si(100) and Ge(100) substrates respectively. It should be noted that as this analysis neglects the 3 nm Ga_2O_3 overlayer, the signal from the bulk Si/Ge is reduced relative to that of the native oxide, the calculated thicknesses are an upper limit, and the actual thickness of the native oxide will be less than this. Whilst, it would be expected that the interfacial oxide may have an effect on the band alignment, the band offsets reported here are consistent with those reported by Chen *et al.*[12] who do not observe the

interfacial native oxide. This would suggest that a thin interfacial oxide, as observed here, has little effect on the band alignment, and hence the device performance.

To summarize, amorphous Ga_2O_3 films are grown on Si and Ge substrates by ALD. The valence band offsets are determined by XPS to be 3.49±0.08 eV, 3.47±0.08 eV and 3.51±0.08 eV for the Si(111), Si(100) and Ge(100) substrates respectively. IPES is also used to investigate the conduction band of a thick Ga_2O_3 film, by combining the IPES with VB-XPS, the band gap is found to be 4.63±0.14 eV. The resulting conduction band offsets are found to be 0.03, 0.05 and 0.45 eV respectively, resulting in a type I heterojunction in all cases. In all cases a thin, native oxide is observed after deposition. The determination of the band alignments to this accuracy, has important implications for devices based on Ga_2O_3/Si and Ga_2O_3/Ge heterojunctions, including MOSFET and MOSCAP type devices.

The authors acknowledge the EPSRC (UK) project no. EP/K014471/1 "Silicon Compatible GaN Power Electronics" for funding.

[1] J. Frank, M. Fleischer, and H. Meixner, Sensors Actuators B Chem. **34**, 373 (1996).

[2] J. Frank, M. Fleischer, and H. Meixner, Sensors Actuators B Chem. **48**, 318 (1998).

[3] C. Baban, Y. Toyoda, and M. Ogita, Thin Solid Films **484**, 369 (2005).

[4] H. Kim, S.-J. Park, and H. Hwang, J. Vac. Sci. Technol. B Microelectron. Nanom. Struct. **19**, 579 (2001).

[5] T. Minami, Y. Nishi, and T. Miyata, Appl. Phys. Express **6**, 044101 (2013).

[6] J. Wen, L.Q. Guo, and J. Tao, IOP Conf. Ser. Mater. Sci. Eng. **170**, 012009 (2017).

[7] D. Guo, Z. Wu, P. Li, Y. An, H. Liu, X. Guo, H. Yan, G. Wang, C. Sun, L. Li, and W. Tang, Opt. Mater. Express **4**, 1067 (2014).

[8] X.Z. Liu, P. Guo, T. Sheng, L.X. Qian, W.L. Zhang, and Y.R. Li, Opt. Mater. (Amst). **51**, 203 (2016).

[9] X.C. Guo, N.H. Hao, D.Y. Guo, Z.P. Wu, Y.H. An, X.L. Chu, L.H. Li, P.G. Li, M. Lei, and W.H. Tang, J. Alloys Compd. **660**, 136 (2016).

[10] A. Paskaleva, D. Spassov, and P. Terziyska, J. Phys. Conf. Ser. **755**, 011001 (2016).

[11] R.L. Anderson, IBM J. Res. Dev. **4**, 283 (1960).

[12] Z. Chen, K. Nishihagi, X. Wang, K. Saito, T. Tanaka, M. Nishio, M. Arita, and Q. Guo, Appl. Phys. Lett. **109**, 1 (2016).

[13] L.K. Chu, T.D. Lin, M.L. Huang, R.L. Chu, C.C. Chang, J. Kwo, and M. Hong, Appl. Phys. Lett. **94**, 10 (2009).

[14] T.W. Pi, M.L. Huang, W.C. Lee, L.K. Chu, T.D. Lin, T.H. Chiang, Y.C. Wang, Y.D. Wu, M. Hong, and J. Kwo, Appl. Phys. Lett. **98**, 2 (2011).

[15] Y. Huang, J.P. Xu, L. Liu, P.T. Lai, and W.M. Tang, IEEE Trans. Electron Devices **63**, 2838 (2016).

[16] E.A. Kraut, R.W. Grant, J.R. Waldrop, and S.P. Kowalczyk, Phys. Rev. Lett. **44**, 1620 (1980).

[17] S.H. Park, S.H. Kim, S.Y. Park, and C. Lee, RSC Adv. **4**, 63402 (2014).

[18] J. Jeong and Y. Hong, IEEE Trans. Electron Devices **59**, 710 (2012).

[19] M. Rebien, W. Henrion, M. Hong, J.P. Mannaerts, and M. Fleischer, Appl. Phys. Lett. **81**, 250 (2002).

[20] M. Passlack, E.F. Schubert, W.S. Hobson, M. Hong, N. Moriya, S.N.G. Chu, K. Konstadinidis, M.L. Schnoes, G.J. Zydzik, J.P. Mannaerts, M.L. Schnoes, and G.J. Zydzik, J. Appl. Phys. **77**, 686 (1995).

[21] M.D. Heinemann, J. Berry, G. Teeter, T. Unold, D. Ginley, M.D. Heinemann, J. Berry, G. Teeter, T. Unold, and D. Ginley, Appl. Phys. Lett. **108**, 1 (2016).

[22] R. O'Donoghue, J. Rechmann, M. Aghaee, D. Rogalla, H.-W. Becker, M. Creatore, A.D. Wieck, and A. Devi, Dalt. Trans. **46**, 16551 (2017).

[23] T. Koida, Y. Kamikawa-Shimizu, A. Yamada, H. Shibata, and S. Niki, IEEE J. Photovoltaics **5**, 956 (2015).

[24] P. de Mierry, D. Ballutaud, and M. Aucouturier, J. Electrochem. Soc. **137**, 2966 (1990).

[25] M.H. Kibel and P.W. Leech, Surf. Interface Anal. **24**, 605 (1996).

[26] P. Gorostiza, R. Díaz, J. Servat, and F. Sanz, J. Electrochem. Soc. **144**, 909 (1997).

[27] A. Rifai, S. Maikap, and Y. Nakamura, J. Vac. Sci. Technol. B **33**, 051812 (2015).

[28] Q. Li, S.J. Wang, K.B. Li, A.C.H. Huan, J.W. Chai, J.S. Pan, and C.K. Ong, Appl. Phys. Lett. **85**, 6155 (2004).

[29] S.J. Wang, A.C.H. Huan, Y.L. Foo, J.W. Chai, J.S. Pan, Q. Li, Y.F. Dong, Y.P. Feng, and C.K. Ong, Appl. Phys. Lett. **85**, 4418 (2004).

[30] M. Perego, G. Seguini, G. Scarel, M. Fanciulli, and F. Wallrapp, J. Appl. Phys. **103**, (2008).

[31] M.P. Seah and W.A. Dench, Surf. Interface Anal. **1**, 2 (1979).

[32] H. Tokutaka, K. Nishimori, and H. Hayashi, Surf. Sci. **149**, 349 (1985).

[33] K. Kakushima, K. Okamoto, K. Tachi, J. Song, S. Sato, T. Kawanago, K. Tsutsui, N. Sugii, P. Ahmet, T. Hattori, and H. Iwai, J. Appl. Phys. **104**, (2008).

[34] S.A. Chambers, Y. Du, R.B. Comes, S.R. Spurgeon, and P. V. Sushko, Appl. Phys. Lett. **110**, 0 (2017).

[35] K.J. Hubbard and D.G. Schlom, J. Mater. Res. **11**, 2757 (1996).

[36] D.G. Schlom and J.H. Haeni, MRS Bull. 198 (2002).

[37] G.B. Alers, D.J. Werder, Y. Chabal, H.C. Lu, E.P. Gusev, E. Garfunkel, T. Gustafsson, and R.S. Urdahl, Appl. Phys. Lett. **73**, 1517 (1998).

[38] H. Ono and K.I. Koyanagi, Appl. Phys. Lett. **75**, 3521 (1999).

[39] T.M. Klein, D. Niu, W.S. Epling, W. Li, D.M. Maher, C.C. Hobbs, R.I. Hegde, I.J.R. Baumvol, and G.N. Parsons, Appl. Phys. Lett. **75**, 4001 (1999).

[40] M. Kundu, N. Miyata, and M. Ichikawa, Appl. Phys. Lett. **78**, 2001 (2001).

[41] R. Puthenkovilakam and J.P. Chang, Appl. Phys. Lett. **84**, 1353 (2004).

[42] Y. Kamata, Y. Kamimuta, T. Ino, and A. Nishiyama, Japanese J. Appl. Physics, Part 1 Regul. Pap. Short Notes Rev. Pap. **44**, 2323 (2005).

[43] R. Zhang, P.C. Huang, J.C. Lin, M. Takenaka, and S. Takagi, Appl. Phys. Lett. **102**, 1 (2013).

[44] G. Hollinger and F.J. Himpsel, J. Vac. Sci. Technol. A Vacuum, Surfaces, Film. **1**, 640 (1983).

[45] G. Hollinger and F.J. Himpsel, Appl. Phys. Lett. **44**, 93 (1984).

[46] W. Ranke and Y.R. Xing, Surf. Sci. **157**, 353 (1985).

[47] D. Schmeisser, R.D. Schnell, A. Bogen, F.J. Himpsel, D. Rieger, G. Landgren, and J.F. Morar, Surf. Sci. **172**, 455 (1986).

[48] J.F. Moulder, W.F. Stickle, P.E. Sobol, and K.D. Bomben, *Handbook of X-Ray Photoelectron Spectroscopy* (Physical Electronics, Inc., Eden Prairie, Minnesota, 1995).

[49] J.M. Hill, D.G. Royce, C.S. Fadley, L.F. Wagner, and F.J. Grunthaner, Chem. Phys. Lett. **44**, 225 (1976).

[50] P.J. Cumpson, Surf. Interface Anal. **29**, 403 (2000).

[51] C.J. Powell and A. Jablonski, J. Electron Spectros. Relat. Phenomena **178**–**179**, 331 (2010).